

# PROGRAMMABLE PHOTONIC FILTERS FABRICATED WITH DEEPLY ETCHED WAVEGUIDES

Erik J. Norberg<sup>†</sup>, Robert S. Guzzon<sup>†</sup>, Steven C. Nicholes<sup>\*</sup>, John S. Parker<sup>†</sup> and Larry A. Coldren<sup>†</sup>

<sup>†</sup>*Department of Electrical and Computer Engineering*  
<sup>\*</sup>*Department of Materials*  
 University of California, Santa Barbara 93106

## Abstract

Novel monolithic programmable optical filters are proposed and demonstrated. Deeply-etched waveguides are used throughout. Unit cells, incorporating a ring resonator in one arm of a Mach-Zehnder, have given programmable poles and zeros; cascaded unit cells have yielded flat-topped band-pass filter characteristics.

## I. Introduction

Programmable optical filters have the potential to improve latency in real-time signal processing applications compared to digital approaches. The idea of programmable optical filters was suggested over two decades ago [1], however their complexity, control, and stability have all been limited by the inability to integrate the optical components on a chip. More recently, channel selection and add/drop multiplexer filters have been shown for WDM applications using micro ring resonators as well as larger ring geometries [2-6]. We propose a family of IIR (infinite-impulse-response) and FIR (finite-impulse response) optical filters that can be constructed from arrays of unit cells that incorporate a ring resonator within one branch of a Mach-Zehnder interferometer (MZI). These can be used as “channelizing” or “matched” filters to prefilter massive amounts of incoming analog data in nearly real time to identify signal bands or signatures that are worthy of further more detailed digital signal processing. This analog filter application is very challenging in that it requires fully programmable filters with much broader wavelength and bandwidth tunability than channel selection filters. Therefore these filters would consist of many sections with many ring resonators. Here we discuss the building blocks of these filters consisting of one and two unit cells.

## II. Material Platform and Waveguide Design

The device design is based on a standard InGaAsP active/passive Offset Quantum Well (OQW) platform with a 300nm 1.3Q waveguide layer and 7 OQWs with a total confinement factor of 7.1% [7]. A single blanket regrowth of p-cladding following active/passive definition was utilized. In order to minimize radiation loss from waveguide bends and simultaneously keep the fabrication as simple as possible, the device uses a deeply etched waveguide design. Fig.1a shows the mode profile for the deep etch design. Since the mode has a large contact area with the waveguide sidewalls, the fabrication of smooth anisotropic sidewalls becomes

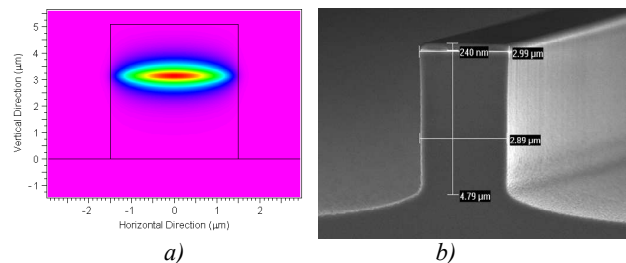


Fig.1 a) Simulated mode profile for deep etched ridge. b) SEM image of deep etched ridge waveguide.

extremely crucial to avoid optical scattering loss and surface recombination currents.

Photolithography and a dual mask process using a 55nm Cr layer on top of 500nm SiO<sub>2</sub> was employed to define the waveguide mask. The deep etching was then carried out in an ICP system using a Cl<sub>2</sub>:H<sub>2</sub>:Ar chemistry and a Si carrier wafer. Previous papers have reported the use of this etch chemistry and the importance of using a Si-carrier for dry etching InGaAsP [8],[9]. In this work the etch conditions were optimized to give anisotropic and smooth sidewalls. Fig.1 shows a cross section of a deep etched waveguide.

Using the cleave-back method on deeply etched active and active/passive ridge lasers, the waveguide loss was extracted, and the results are summarized in Table 1. Both the loss numbers and threshold current densities are very encouraging. Comparing the passive loss to that of 3μm surface ridges formed with a crystallographic wet etch (1.9 cm<sup>-1</sup> measured) suggests that there is not significant scattering loss added from the sidewalls. The low threshold current densities for the 3μm ridges confirm that the surface recombination current at the

Table.1 Loss coefficients and threshold current data for deeply etched waveguides measured under pulsed conditions.

Ridge width [μm]	$\alpha_i$ [cm <sup>-1</sup> ]	$\alpha_p$ [cm <sup>-1</sup> ]	Threshold current density / well [A/cm <sup>2</sup> ], (Laser length>1500μm)
3.0	8.5	2.2	75.7±7.8
1.8	11.4	-	129±12.4

sidewalls is not a major issue for this ridge width. However, the higher threshold current densities for the narrower 1.8 $\mu\text{m}$  ridges imply a larger portion of the injected current goes into surface recombination. For this reason, all active gain sections in the device design have waveguides of 3 $\mu\text{m}$ ; while the waveguide is tapered down to 1.8 $\mu\text{m}$  at the input of couplers to reduce the coupling length.

Gain measurements from deeply etched SOAs show large signal gains of about 260 dB/cm (60 cm<sup>-1</sup>) with an output 1-dB saturation of 8.4 dBm. This gain is about 25% higher than what we have seen using the same OQW platform with surface ridge waveguides of the same width.

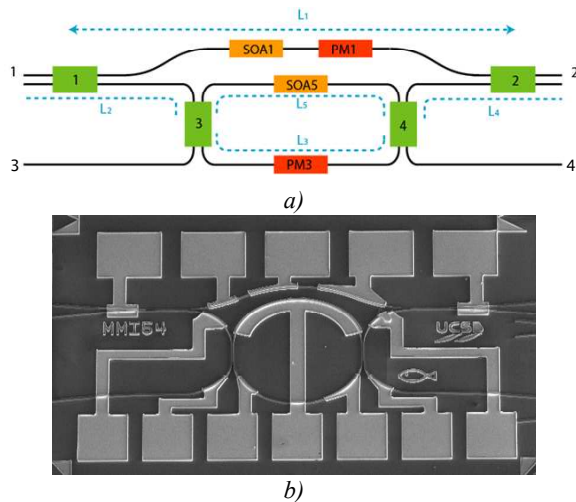


Fig.2 a) Schematic and b) SEM picture of the Single Ring Unit cell.

### III. Device Design

#### A. Single Ring Unit Cell

The simplest filter design incorporates one ring and a parallel “feed-forward” waveguide. This is the Single Ring Unit Cell, shown fabricated in the SEM picture, Fig.2b; a schematic drawing is also shown in Fig.2a. When a signal is input to port 1, it encounters two interfering branches, one of which contains a ring resonator. A first-order pole response is created by the ring. A first-order zero response is created by the Mach-Zehnder Interferometer that is formed from the independent paths of the ring and the feed-forward waveguide. Thus, FIR and IIR filter responses can be synthesized between ports 1 and 2 as well as between other pairs of ports. The response of this unit cell is tuned in amplitude via active SOA regions in each path. The phase is tuned by carrier injection into passive waveguide sections via the free-carrier-absorption effect. We have formulated the scattering parameters for the single ring unit cell, shown here in a simplified form for an input to port 1 and an output at port 2.

$$S_{21} = AG_{ff}e^{-j(\beta L_1 + \Phi_{ff})} + \frac{Be^{-j[\beta(L_2 + L_3 + L_4) + \Phi_{ring}]}}{1 - CG_{ring}e^{-j[\beta(L_3 + L_5) + \Phi_{ring}]}} \quad (1)$$

The A, B, and C coefficients include the loss from various elements in the structure including waveguide, MMI transmission, and MMI coupling loss.  $G_{ff}$  and  $G_{ring}$  are the gain provided by the SOA for the feed-forward and ring respectively. The response of the zero can be isolated by applying a reverse bias to the SOA in the ring, and likewise the response of the pole can be isolated by applying a reverse bias to the SOA in the feed-forward waveguide.

In the fabricated device, the resonator has a length of 915 $\mu\text{m}$  and the length difference of the MZI arms is 330 $\mu\text{m}$ , corresponding to an FSR of 0.7nm (87GHz) and 2nm (249GHz) respectively. In addition to the active SOAs and passive phase tuning pads, a number of short passive pads or “taps” were included, Fig.2b. By reverse biasing these taps in different places along the unit cell, the individual components can be better understood. By calibrating the quantum efficiency of the taps using separate test structures, the taps can ultimately be used as sensors which together with feed-back loops can stabilize the filter operation.

#### B. Cascaded Unit Cells

When two single ring unit cells are cascaded, a system with 3 coupled rings is created. The transfer function of this system has 6 total poles. 3 are created by individual rings, while 3 are manifest in the coupling between rings. 2 of the coupling poles are formed by the “figure-eight” path formed by 2 rings, and 1 is created by the similar combination of 3 rings. Cascaded coupled ring unit cells were fabricated together with the single ring unit cells, shown in Fig. 3. The fabricated device has a resonator length of 1500 $\mu\text{m}$ . The design – like the Single Ring Unit Cell – includes passive contacts that act as phase modulators or “taps.”

The possibilities for the response from the coupled ring system is great, as the poles and zeros can be tuned via the SOAs and phase modulators. In general, many unit cells can be cascaded, allowing for the synthesis of complex filters. For example, a flat-topped bandpass response of any order can be synthesized for an input to port 1 and an output at port 2 by applying a reverse bias to the feed-forward SOAs (SOA1 in the schematic), and applying a forward bias the ring SOAs. This coupled-ring bandpass filter could be suitable for WDM add/drop filter applications [3]. To synthesize a narrow bandwidth filter, reverse and forward biases are applied to the SOAs in alternating rings, effectively cascading the poles from every other ring. For example in our 3-ring system, this is accomplished by reverse biasing the SOA in the center ring. With the rings no longer coupled, their poles can be located at the same wavelength to create a sharp filter response. The MZI structures created by the feed-forward waveguides can be tuned to eliminate neighboring poles and improve the effective FSR of the filter.

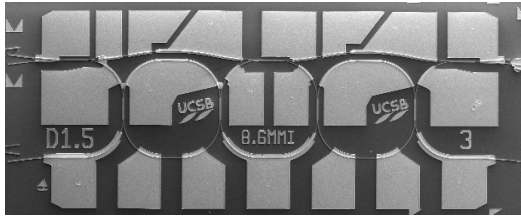


Fig.3 SEM of a Cascaded Unit Cell including 3 coupled rings.

## IV. Results

### A. Single Ring Unit Cell

Measurements of the filters were made by fiber coupling broadband light from an Amplified Spontaneous Emission (ASE) source into the chip and fiber coupling the output into an Optical Spectrum Analyzer (OSA). All testing was performed CW at room temperature. An MZI response was generated by reverse biasing the ring SOA to -9V to shut off the resonator; the feed-forward SOA was also reversed biased at -4V in order to balance the coupling loss induced by the path going through the resonator. The resulting MZI zero shows an extinction ratio of 15dB, and the  $S_{21}$  simulation (1) was fitted with  $AG_{ff}=0.8B$ ,  $G_{ring}=0$ , Fig. 4a. The pole response was measured between ports 3 & 4 with the ring SOA biased at 17mA ( $I_{th}=20mA$ ), resulting in an extinction ratio of 15dB with a pole FWHM of 0.067nm (8.5GHz), corresponding to a resonator Q-value of 23,000, as shown in Fig. 4b. Simulations fits a pole value of  $CG_{ring}=0.76$  with  $G_{ff}=0$ .

### B. Cascaded Unit Cells

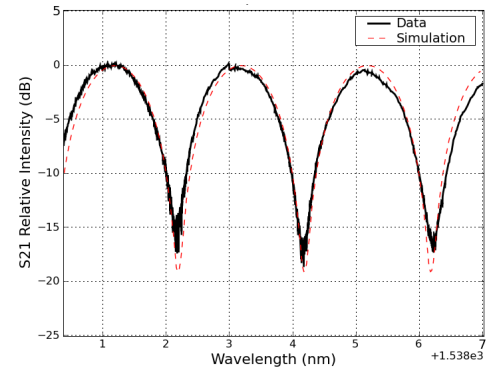
Fig. 5 shows a simple 2<sup>nd</sup>-order pole response measured from the device illustrated in Fig. 3. This was created by turning off the feed-forward waveguides and the third ring by applying a reverse bias to their respective SOAs; the remaining two 2 rings were tuned to create a band-pass filter with a 0.302 nm (37.7 GHz) FWHM. Given the strong 3 dB interstage coupling in this filter, a relatively wide-bandwidth, low-extinction passband results.

## IV. Conclusion

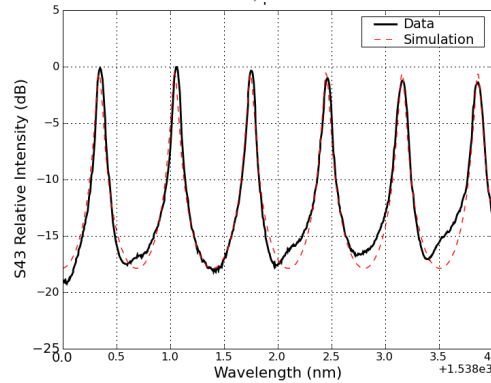
We have designed and fabricated the building blocks for a novel programmable filter entirely based on deep etching. By optimizing ICP etch conditions in  $Cl_2:H_2:Ar$  chemistry we have achieved low loss passive waveguides and high active gain. Basic filter characteristics are demonstrated, including a high-Q single-ring-resonator pole response and a MZI zero response. By monolithically cascading unit cells, a band-pass filter was realized.

## Acknowledgements

This work was supported by the DARPA-PhASER Project. A portion of this work was done in the UCSB nanofabrication facility, part of the NSF funded NNIN network.



a)



b)

Fig.4 Measured Single Unit Cell responses with superimposed  $S_{21}$  simulations using (1). a) MZI zero response; b) Resonator pole response.

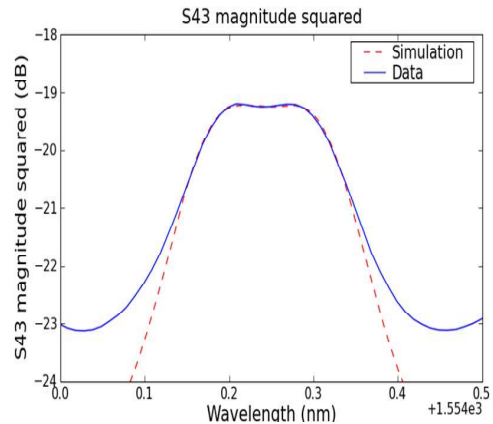


Fig.5 Measured and simulated throughput from 2-coupled-ring bandpass filter tuned to ~ 0.1 dB ripple with a 0.302 nm (37.7 GHz) FWHM.

## References

- [1] J. E. Bowers, S. A. Newton, W. V. Sorin, and H. J. Shaw, "Filter Response of Single Mode Fiber Recirculating Delay Lines," *Elec. Letts*, **18**, 110, (1982).
- [2] S. Matsuo, Y. Ohiso, K. Tateno, T. Segawa, M. Kohtoku,

and S. Oku, "A high-speed tunable optical filter using a semiconductor double-ring resonator," *IPRM*, 14th, 467-470, (2002).

[3] D. Rabus, M. Hamacher, U. Troppenz, and H. Heidrich, "Optical filters based on ring resonators with integrated semiconductor optical amplifiers in GaInAsP-InP," *JSTQE*, **8**, 1405-1411(2002).

[4] S. Choi, Z. Peng, Q. Yang, E. H. Hwang, and P. Dapkus, "A high-Q wavelength filter based on buried heterostructure ring resonators integrated with a semiconductor optical amplifier," *IEEE Photonics Technology Letters*, **17**, 2101-2103 (2005).

[5] A. Agarwal et al. "Fully programmable ring-resonator-based integrated photonic circuit for phase coherent applications," *J. Lightwave Technology*, **24**, 77-87 (2006).

[6] Y. Ma, S. Chang, S. Chang, and S. Ho. "Improved optical filter responses in cascaded InGaAsP/InP microdisk resonators," *Electronics Letters*, **37**, 564-565 (2001).

[7] E. J. Skogen, J. W. Raring, G. B. Morrison, C. S. Wang, V. Lal, M. L. Masanovic, and L. A. Coldren, "Monolithically integrated active components: a quantum-well intermixing approach," *IEEE JSTQE*, **11** (2), 343-355, (2005).

[8] Sean L. Rommel, "Effect of H<sub>2</sub> on the etch profile of InP/InGaAsP alloys in Cl<sub>2</sub>/Ar/H<sub>2</sub> inductively coupled plasma reactive ion etching chemistries for photonic device fabrication," *J. Vac. Sci. Technol. B*, **20** (4), (Jul/Aug 2002).

[9] S. Bouchoule et al., "Sidewall passivation assisted by a silicon coverplate during Cl<sub>2</sub>-H<sub>2</sub> and HBr inductively coupled plasma etching of InP for photonic devices," *J. Vac. Sci. Technol. B*, **26** (2), (Mar/Apr 2008).